Inorganic Chemistry

Article

pubs.acs.org/IC

Crystal Structure and Magnetic Properties of the $S = {}^1/_2$ Quantum Spin System $Cu_7(TeO_3)_6F_2$ with Mixed Dimensionality

Shichao Hu,[†] Amber Mace,[†] Mats Johnsson,*[,†] Vladimir Gnezdilov,[‡,§] Peter Lemmens,[‡] Joshua Tapp,[∥] and Angela Möller[∥]

[†]Department of Materials and Environmental Chemistry, Stockholm University, SE-106 91 Stockholm, Sweden

[‡]Institute for Physics of Condensed Matter, TU Braunschweig, D-38106 Braunschweig, Germany

[§]B. I. Verkin Institute for Low Temperature Physics and Engineering of the National Academy of Sciences of Ukraine, Kharkov 61103, Ukraine

[∥]Department of Chemistry and Texas Center for Superconductivity, University of Houston, 112 Fleming Building, Houston, Texas 77204-5003, United States

Supporting Information

ABSTRACT: The new oxofluoride $Cu_7(TeO_3)_6F_2$ has been synthesized by hydrothermal synthesis. It crystallizes in the triclinic system, space group $P\bar{1}$. The crystal structure constitutes a Cu−O framework with channels extending along [001] where the F^- ions and the stereochemically active lone-pairs on Te^{4+} are located. From magnetic susceptibility, specific heat, and Raman scattering measurements we find evidence that the magnetic degrees of freedom of the Cu−O−Cu segments in $Cu_7(TeO_3)_6F_2$ lead to a mixed dimensionality with single Cu $S = {}^1/_2$ moments weakly coupled to spin-chain fragments. Due to the weaker coupling of the single moments, strong fluctuations exist at elevated temperatures, and long-range magnetic ordering evolves at comparably low temperatures (T_N = 15 K).

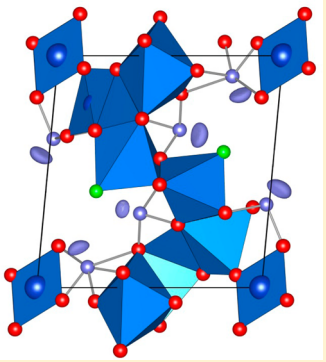

INTRODUCTION

The p-block cations with ns^2np^0 electronic configurations, e.g., Te^{4+}, Se^{4+}, and Sb^{3+}, usually display a stereochemically active lone electron pair and adopt an asymmetric or one-sided coordination to anion ligands. The lone-pair electrons do not participate in the bonding but occupy a volume similar to that of an oxide. They can therefore be regarded as an additional ligand that stabilizes asymmetric coordinations.[1−3] In addition, the halide ions in the M−L−O−X family (M = transition metal cation; L = p-block lone-pair elements such as Te^{4+}, Se^{4+}, or Sb^{3+}; X = Cl or Br) also play an important role in reducing the dimensionality of a crystal structure due to the different bonding preferences between the transition metal and lone-pair cation; that is, the late transition metal cations prefer to bond with both oxygen and halide anions while for lone-pair cations exclusive coordination to oxygen anions is preferred. In previous studies it has been found that chloride/bromide ions usually show low coordination numbers and act as terminating species that reside together with the lone-pairs in large voids in the crystal structure. Several compounds presenting this feature of low-dimensional arrangements of transition metal cations and even quantum spin systems with interesting magnetic properties have been reported.[4−9] In particular the compound $Cu_2Te_2O_5X_2$ that is composed of weakly coupled spin tetrahedra and $FeTe_2O_5X$ exhibiting multiferroicity have received considerable attention.[10,11] Much less attention has been paid to the M−L−O−F system thus far due to difficulties with synthesizing such compounds and due to the fluorine normally acting as a framework builder and not as a terminating ion. The literature on oxofluorides is still not extensive, and the number of oxofluorides containing lone-pair elements is very limited. However, it is reasonable to assume that a rich variety of new compounds could be discovered in the M−L−O−F system. Recently Laval et al. have performed systematic work on exploring the M−L−O−F system with Te^{4+}, and some interesting compounds have been found, e.g., $MTeO_3F$ (M = Fe, Cr, Ga, In, Sc),[12,13] $V_2Te_2O_7F_2$,[14] $TiTeO_3F_2$,[14] and $InTe_2O_5F$;[15] however, only minor amounts of those compounds have been synthesized, and their physical properties have not been investigated. We recently found the first two cobalt oxofluorides comprising lone-pair elements, $Co_2TeO_3F_2$ and $Co_2SeO_3F_2$.[16] The role of fluorine in all those compounds is, as expected, to be framework builders like oxygen instead of being a terminating ion as chlorine and bromine.

In this Article, we report the new synthetic compound, $Cu_7Te_6O_{18}F_2$, which to our best knowledge is the first copper based oxofluoride in the M−L−O−F family and also a compound with $S = {}^1/_2$ moments weakly coupled to a spin chain. The fluorine herein acts as a terminating species.

Received: April 25, 2014
Published: June 23, 2014

   dx.doi.org/10.1021/ic5009686 | Inorg. Chem. 2014, 53, 7661−7667

EXPERIMENTAL SECTION

Single crystals of $Cu_7(TeO_3)_6F_2$ were prepared by hydrothermal synthesis. A mixture of 0.223 g (2.2 mmol) of CuF_2 (Aldrich, 99.9%) and 0.160 g (1.0 mmol) of TeO_2 (Alfa Aesar 99%) together with 2 mL of deionized water was sealed in a 23 mL Teflon lined steel autoclave and heated to 230 °C for 3 days. Green block-like single crystals with an average size of ca. 0.25 × 0.1 × 0.05 mm^3 were separated from unreacted TeO_2 in an ultrasonic bath and subsequently selected and washed using water and ethanol followed by drying at room temperature. The chemical compositions of the products were analyzed by using a scanning electron microscope (SEM, JEOL JSB-7000F) equipped with an energy-dispersive spectrometer (EDS).

Single-crystal X-ray data were collected at 293 K on an Oxford Diffraction Xcalibur3 diffractometer using graphite-monochromatized Mo Kα radiation, λ = 0.710 73 Å. Data reduction and absorption corrections were made using the software CrysAlis RED[17] provided by the diffractometer manufacturer. The crystal structure was solved by direct methods using the program SHELXS-97 and refined by full matrix least-squares on F^2 using the program SHELXL-97.[18] The product purity was confirmed by comparing the experimental X-ray powder diffraction pattern, obtained with a Panalytical X'Pert PRO diffractometer, with a simulated pattern from the crystal structure. All atoms were refined with anisotropic displacement parameters. Details of the final refinement are shown in Table 1. Further details on the crystal structural investigations can be obtained from the Fachinformationszentrum Karlsruhe, Abt. PROKA, 76344 Eggenstein-Leopoldshafen, Germany (fax +49-7247-808-666; e-mail crysdata@fiz-karlsruhe.de) on quoting the following depository number: CSD-427315. The structural drawings are made with the program VESTA.[19] Bond valence sum calculations (BVS) were made using the following R_0 values: 1.977 for Te−O bonds, 1.679 for Cu−O bonds, and 1.594 for Cu−F bonds.[20]

Electron localization function (ELF) values for the stereochemically active lone-pairs were calculated using the CP2K software[21] by performing a DFT energy calculation on one unit cell of the structure with periodic boundary conditions implemented. CP2K performs periodic plane wave DFT calculations "on the fly" utilizing the GPW method[22] implemented by the QUICKSTEP module. In the calculations, only the valence electrons are treated explicitly, for which the wave functions are modeled by the DZVP-MOLOPT-SR basis set while the core electrons are modeled effectively, for each atom, with the GTH pseudopotential.[23] The DFT-D3 vdW correction term by Grimme et al.[24] was used. The calculated lone-pair regions were presented by visualizing isosurfaces with ELF-value η = 0.9 using the VESTA software.[19]

Magnetic susceptibility and specific heat were investigated on a powder pellet using a physical property measurement system (PPMS, Quantum Design). Magnetic susceptibility has been investigated using field cooled (FC) as well as zero field cooled (ZFC) experiments in magnetic fields of 0.1 T. The data were corrected for diamagnetic contributions.[25] Raman scattering experiments were performed on small single crystals using a triple spectrometer (Dilor XY500, Horiba) with 532 nm laser excitation as a function of temperature.

Table 1. Crystal Data and Structure Refinement Parameters for $Cu_7(TeO_3)_6F_2$

empirical formula	$Cu_7(TeO_3)_6F_2$
fw	1536.38
T (K)	293(2)
wavelength (Å)	0.710 73
cryst syst	triclinic
space group	$P\bar{1}$
a (Å)	4.9844(2)
b (Å)	9.4724(4)
c (Å)	9.9580(4)
α (deg)	82.318(4)
β (deg)	76.275(4)
γ (deg)	78.847(4)
V (Å^3)	446.20(3)
Z	1
density$_{calcd}$ (g cm^{-3})	5.717
F(000)	677
cryst color	green
cryst habit	block
cryst size (mm^3)	0.25 × 0.09 × 0.03
θ range for data collection (deg)	3.19−28.66
index ranges	$-6 \le h \le 6$
	$-12 \le k \le 12$
	$-13 \le l \le 13$
reflns collected	4987
indep reflns	2002 [R(int) = 0.0188]
data/restraints/params	2002/0/152
refinement method	full-matrix least-squares on F^2
GOF, S	1.031
final R indices [$I > 2\sigma(I)$][a]	R1 = 0.0167
	wR2 = 0.0400
R indices (all data)	R1 = 0.0182
	wR2 = 0.0405

[a] $R1 = \sum||F_o| - |F_c||/\sum|F_o|$; $wR2 = \{\sum[w(F_o^2 - F_c^2)^2]/\sum[w(F_o^2)^2]\}^{1/2}$.

RESULTS

Crystal Structure. The new compound $Cu_7(TeO_3)_6F_2$ crystallizes in the triclinic system, space group $P\bar{1}$, see Table 1. The chemical composition was analyzed using energy-dispersive spectrometry (EDS). Quantitative analysis confirms the presence of all the elements Cu:Te:O:F. The elements Cu and Te were analyzed quantitatively and are present in a ratio that is close to the result from the crystal structure refinement, see Supporting Information Table S4.

The crystal structure constitutes a framework with non-bonding channels extending along [001] where the F^- ions and the stereochemically active lone-pairs on Te^{4+} are located, see Figure 1a. We have not found other examples of oxofluorides where fluorine is a terminating ion in contrast to the common functionality as a framework building ion like oxygen as in, e.g., $ScPbO_2F$,[26] $NbBi_2O_5F$,[27] and VBi_2O_5F.[28] Bond valence sum (BVS) calculations support that the Cu, Te, and O ions have the charges +2, +4, and +2, respectively. However, the BVS for fluorine is only 0.39 as a consequence of it being a terminating ion, which is significantly lower than values normally observed for oxofluorides, e.g., 0.92 in $Co_2Se_2O_3F_2$[16] and 0.83 in $FeTeO_3F$.[12] On the other hand, BVS values substantially lower than 1.0 for Cl and Br are very common for compounds of the M−L−O−X (M = late transition metal, L= p-element lone-pair cation, X = Cl, Br) family, where Cl or Br frequently are terminating ions in the crystal structure, e.g., 0.34 for Cl in $Ca_2Fe_6(SeO_3)_9Cl_4$,[29] and 0.66 for Br in $CoSb_2O_3Br_2$.[30]

There are in total four crystallographically different copper atoms with variable coordination. Cu(1) is the only atom located on a special position which is the inversion center at the corner of the unit cell. Cu(1) is coordinated to O(3) and O(2) with Cu−O bond distances of 1.903(2) and 1.961(3) Å, respectively, resulting in a distorted square-planar arrangement, [$Cu(1)O_4$]. Cu(2) is bonded to five oxygen atoms resulting in a distorted [$Cu(2)O_5$] square pyramid where O(1), O(3), O(4), and O(9) form the square basis with Cu−O distances in the range 1.916(3)−1.973(3) Å. O(8) constitutes the apex of the pyramid at a distance of 2.373(3) Å. Cu(3) is surrounded

dx.doi.org/10.1021/ic5009686 | Inorg. Chem. 2014, 53, 7661−7667

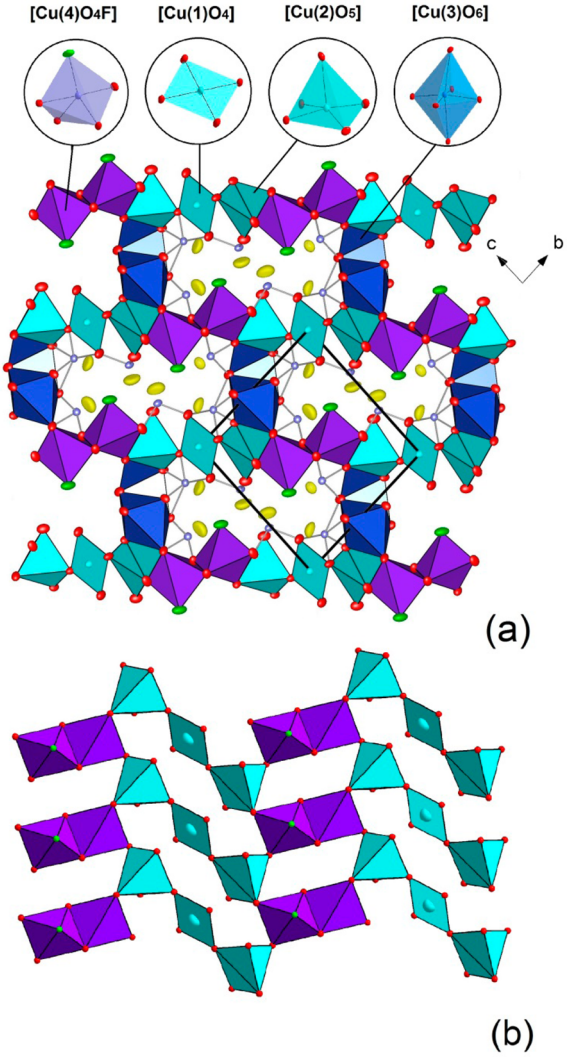

Figure 1. (a) Overview of the crystal structure for $Cu_7(TeO_3)_6F_2$. Four different Cu-coordination polyhedra connect to form the framework. Channels of nonbonding volumes extend along [001] where the F^- ions and the stereochemically active lone-pairs on Te^{4+} reside. The lone-pair positions are calculated with ELF and marked in yellow. (b) Cu−O−F slab parallel to (011).

by six oxygen atoms to form a $[Cu(3)O_6]$ distorted octahedron, with four Cu−O bonds to O(1), O(5), and 2×O(7) in the square plane within the range from 1.948(3) to 1.996(3) Å. The two longer bonds to O(8) and O(5) are 2.544(3) and 2.639(3) Å, respectively. Cu(4) forms a distorted $[Cu(4)O_4F]$ trigonal bipyramid where the F atom is located in the triangular plane. The Cu−F bond distance is 1.938(3) Å, and the bonds to O(8) and O(6) in the triangular plane are 2.034(3) and 2.164(3) Å, respectively, while the two oxygen atoms, O(4) and O(6), at the apexes of the bipyramid have shorter bonding distances 1.916(3) and 1.960(3) Å, respectively.

The $[Cu(3)O_6]$ octahedra are connected to each other by trans-edge sharing in the equatorial position. Two $[Cu(4)_2O_6F_2]$ connect via edge sharing (axial−equatorial) to form an inversion symmetry related $[Cu(4)_2O_6F_2]$ dimer. $[Cu(1)O_4]$ connects via corner sharing to two $[Cu(2)O_5]$ pyramids forming a $[Cu(1)Cu(2)_2O_{12}]$ trimer with the angle Cu(2)−Cu(1)−Cu(2) being 180°. Such trimers are further connected to $[Cu(4)_2O_6F_2]$ dimers via corner sharing resulting in the two-dimensional Cu−O−F slab parallel to (011), see Figure 1b. Those slabs are connected via the longer axial ligands of the $[Cu(3)O_6]$ units along [100] resulting in the Cu−O−F framework, see Figure 1a.

The three crystallographically different Te^{4+} cations all have asymmetric one-sided coordinations. Te(2) and Te(3) are both three-coordinated to oxygen forming $[TeO_3E]$ pseudotetrahedra; this is the most common coordination polyhedron for Te^{4+}, where E designates the stereochemically active lone-pair electrons. The Te−O distances in these tetrahedra are in the range 1.851(3)−1.894(3) Å. The distances from Te(2) and Te(3) to the highest ELF values for the lone-pair are 1.0 and 0.9 Å, respectively. Te(1) has three short Te−O bonds to O(1), O(3), and O(7) in the range, 1.892(2)−1.921(3) Å and additionally shows two longer bonds to O(2) and O(5) at 2.577(6) and 2.489(3) Å, respectively. The latter values result in BVS values of 0.20 and 0.25, indicating that also those two oxygens should be considered as belonging to the primary coordination sphere.[31] Thus, the Te(1) coordination sphere resembles a highly distorted $[TeO_5E]$ octahedron. The distance from Te(1) to the highest ELF value for the lone-pair is 1.0 Å. The three Te-coordination polyhedra polymerize via corner sharing to form $[Te_3O_9E_3]$ groups, see Figure 2, that are further connected to the Cu−O−F framework so that the stereochemically active lone-pairs on Te^{4+} are located in channels in the crystal structure, see Figure 1a.

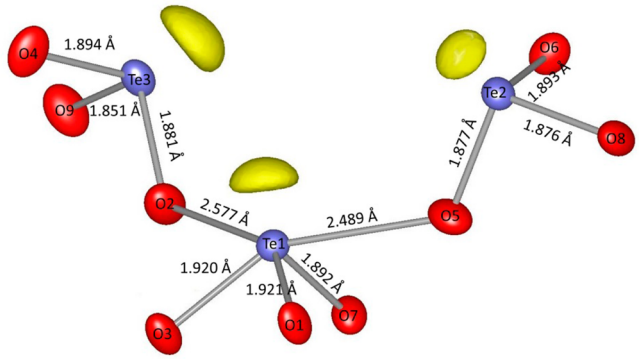

Figure 2. Three Te-coordination polyhedra polymerize via corner sharing to form $[Te_3O_9E_3]$ groups. The lone-pair positions are calculated with ELF and marked in yellow; the distances in between the Te atoms and the highest ELF values are in the range 0.9−1.0 for the different Te atoms.

In the following we will show thermodynamic as well as Raman scattering data to investigate the structure−property relationships for this compound. The data will be analyzed within a scheme of low-dimensional, magnetic superexchange that contains chain elements as well as weakly coupled single, fluctuating spins. Due to the coupling of these two different elements, aspects of long-range magnetic order as well as short-range suppression of fluctuations develop as a function of temperature in a, to our knowledge, unprecedented way.

Thermodynamic Data. The magnetic susceptibility of $Cu_7(TeO_3)_6F_2$ shows a Curie−Weiss behavior at high temperatures with dominant antiferromagnetic interactions. We derive a Curie−Weiss temperature of Θ_{CW} = −368 K, as shown in Figure 3, from the inverse susceptibility. There is no difference between ZFC and FC measurements in 0.1 T in the overall temperature range. Therefore, we may neglect spin canting and strong anisotropies and assume isotropic, antiferromagnetic

dx.doi.org/10.1021/ic5009686 | Inorg. Chem. 2014, 53, 7661−7667

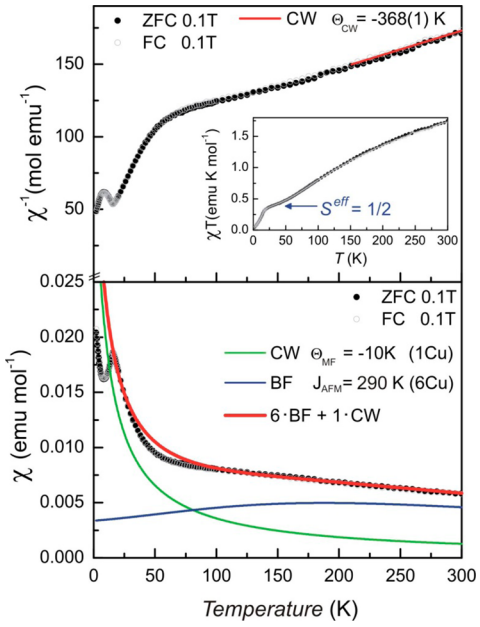

Figure 3. (Top) Inverse magnetic susceptibility of $Cu_7(TeO_3)_6F_2$ in FC and ZFC mode in 0.1 T (open/full circles). At high temperatures the data is shown together with a Curie–Weiss fit (red curve) with Θ_{CW} = −368 K. (Inset) Magnetic susceptibility multiplied by temperature, $\chi \cdot T$. At low temperatures the data shows a plateau consistent with an effective $S^{eff} = {}^1/_2$ moment marked by an arrow. (Bottom) Magnetic susceptibility with fits to a Bonner–Fisher expression for a spin chain (blue) with J_{AFM} = 290 K scaled to 6 spins, a contribution of a weakly coupled $S^{eff} = {}^1/_2$ moment (green) with Θ_{MF} = −10 K, and the sum of both (red).

Heisenberg superexchange of $S = {}^1/_2$ moments as a primary source of magnetism in $Cu_7(TeO_3)_6F$. Up to this point the phenomenology is similar to many compounds containing M = Cu^{2+} ions. However, there are pronounced deviations from the Curie–Weiss behavior at lower temperatures. The inverse susceptibility, χ^{-1}, gradually curves down; i.e., there is a larger moment developing compared to the high-temperature Curie–Weiss behavior. At low temperatures, there exists a dip at $T_N \approx$ 15 K indicative for possible long-range order. The magnitude of the latter effect is comparably small. For $T < T_N$ the inverse susceptibility decreases further to lower temperatures. In $\chi \cdot T$ the temperature evolution of the spin moments is also clearly visible, see inset to Figure 3. In addition, there is a plateau in the temperature regime 30 K < T < 75 K that corresponds to an effective moment of $S^{eff} = {}^1/_2$. This moment must be coupled weaker to the remaining magnetic system as the slopes in $\chi \cdot T$ above and below the above-mentioned temperature regime are different.

To better understand the observed behavior and its relation to the coordinations described above we have fitted the magnetic susceptibility in the bottom part of Figure 3 to a modified Bonner–Fisher model. The Bonner–Fisher model gives an analytic expression of the susceptibility of a strictly one-dimensional arrangement of quantum spins that interact with each other's neighbors by antiferromagnetic Heisenberg exchange interaction, J_{AFM}.[31] It has been derived from calculations of spin-chain segments with increasing length and number of interacting spins. These segments resemble the Cu–O–Cu fragments of $Cu_7(TeO_3)_6F$, shown in Figure 1. Such a magnetic system does not show long-range order. Instead, there is a gradual increase of the inverse magnetic susceptibility around ≈185 K; see also the broad maximum in $\chi(T)$ corresponding to the strength of the coupling of the spins along the chain, $T_{max} \propto 0.64 \cdot J_{AFM}$. A further soft decrease in χ^{-1} occurs at lower temperatures (below ≈75 K). As there exists evidence from $\chi \cdot T$ for an additional effective $S^{eff} = {}^1/_2$ moment that is weakly coupled to the chain and no low-temperature decrease is observed in $\chi(T)$, we use a modeling with an additional spin moment $\chi \propto 1/(T - \Theta_{MF})$ added to the overall chain contribution. The molecular field parameter, Θ_{MF}, mimics the coupling of this moment to the chains. The overall agreement of this fit to the experimental data is surprisingly good, considering that the Bonner–Fisher formula has only the exchange coupling in the chain, here J_{AFM} = 290 K (202 cm^{-1}), as a free parameter (a typical value, g = 2.09, for Cu^{2+} in an oxide coordination is used). The latter coupling constant is in reasonable agreement with $\Theta_{CW} \approx z \cdot J$, taking the coordination number z = 2 for a chain. Furthermore, the fit leads to Θ_{MF} = −10 K, a reasonable magnitude of coupling as the proposed scenario for $Cu_7(TeO_3)_6F_2$ only makes sense with a pronounced hierarchy of interactions, i.e., $\Theta_{MF} \ll J$.

As the small coordination number in one dimension allows pronounced fluctuations, an idealized chain system does not show long-range magnetic ordering. In real systems additional interactions to other spins or to the lattice usually lead to magnetic transitions or a nonmagnetic, dimerized state. It is therefore important to confirm the evidence for long-range magnetic ordering in the bulk as well as to derive its contribution to the magnetic entropy. With this information it is possible to judge to which extent spin moments are still fluctuating for temperatures $T_N < T < \Theta_{CW}$ and whether the anticipated weakly coupled spin moments induce the ordering process.

The specific heat of $Cu_7(TeO_3)_6F_2$ divided by temperature, C_p/T, together with an estimation of the transition induced magnetic specific heat and entropy is shown in Figure 4. As there is no nonmagnetic, isotypic compound known, we approximated the phonon (lattice) part of the specific heat below 50 K where strong fluctuations are suppressed, see Raman data below, and an effective magnetic moment develops, see inset Figure 3. After subtracting a baseline from the specific heat data that approximates its evolution adjacent to the λ-anomaly, we derive a magnetic entropy of only $\Delta S_m \approx R \ln(2)$ = 5.76 J/mol K. This magnitude is much smaller than expected from all Cu moments; i.e., it corresponds to approximately one $S^{eff} = {}^1/_2$ moment only. This observation agrees with the magnetic moment of the plateau in $\chi \cdot T$ that forms in the temperature range 30 K < T < 75 K, see above.

As the high-temperature Curie–Weiss constant, which is an average over all existing exchange constants, is very large, especially larger that T_N, we can assume two properties of the magnetic system: (i) The majority of spin moments are coupled with a large exchange coupling. However, their geometrical arrangement is not consistent with the expected long-range ordering at $T \approx \Theta_{CW}$. (ii) The entropy of these spins is gradually frozen out, distributed over a similar large temperature range, $\Delta T \approx \Theta_{CW}$, and not visible at $T = T_N$. Correspondingly, the observed entropy below 50 K is attributed to a spin moment with a weaker coupling. Even more, the latter moments induce the three-dimensional ordering.

Raman Scattering Data. Raman scattering data of $Cu_7(TeO_3)_6F_2$ as a function of temperature are shown in Figure 5. In good agreement with the expected 48 Raman-

dx.doi.org/10.1021/ic5009686 | Inorg. Chem. 2014, 53, 7661–7667

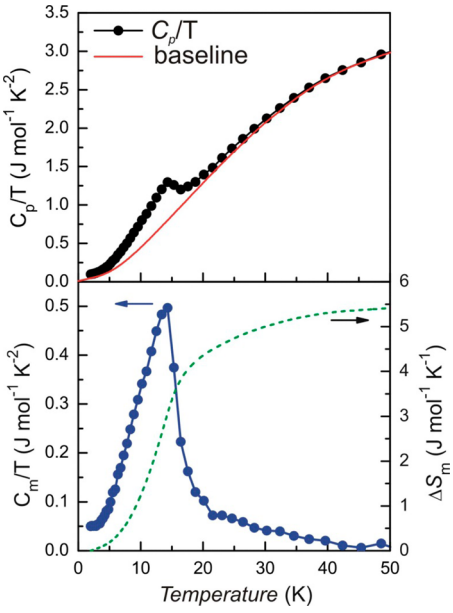

Figure 4. (Top) Specific heat of $Cu_7(TeO_3)_6F_2$ divided by temperature (dots) together with a baseline (red curve) that approximates its evolution adjacent to the lambda-anomaly at $T_N \approx 15$ K. (Bottom) Derived magnetic contribution to the specific heat (blue) and derived entropy (dashed) released at the magnetic transition.

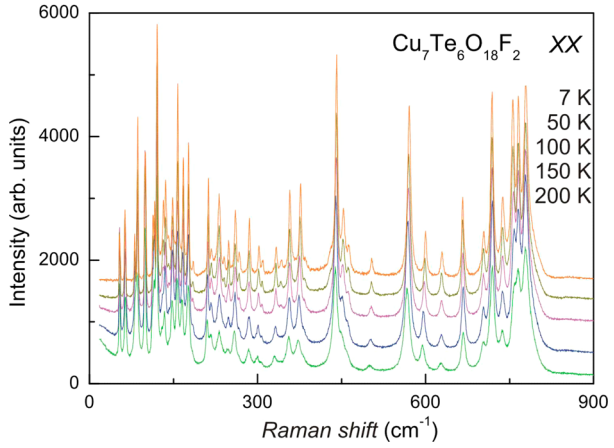

Figure 5. Raman scattering data of $Cu_7(TeO_3)_6F_2$ at selected temperatures showing numerous phonon lines and a continuum of scattering at low energies that decreases in intensity with decreasing temperatures.

active A_g modes from symmetry considerations, we observe a very large number of modes that partly overlap in the frequency range from 50 to 800 cm^{-1}. At low energy there exists a broad, quasielastic scattering continuum with energies $0 < \Delta\omega < 200$ cm^{-1}. This continuum is evident at high temperatures and gradually decreases in intensity for temperatures below 150 K. The temperature evolution of this intensity and its line width are completely different from the phonon scattering. Similar continua with such temperature dependence are observed in compounds with low-dimensional spin arrangements, e.g., in $CuGeO_3$.[33,34] The intensity of the continuum is attributed to fluctuations of the magnetic energy density. The integrated scattering intensity divided by T^2 can be related to the temperature dependence of the magnetic contribution to the specific heat, $C_p(T) \propto I_{Int}(T)/T^2$.

The temperature dependence of four anomalous phonons of $Cu_7(TeO_3)_6F_2$ is shown in Figure 6. There is a moderate

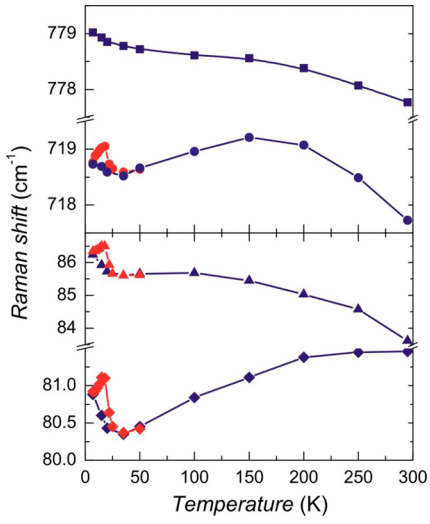

Figure 6. Phonon frequency as a function of temperature (dots) showing a moderate softening of four phonon lines and a hysteresis between cooling (blue) and heating (red) with an onset for $T < 30$ K.

softening of the phonon frequency with an onset for temperatures between 150 and 200 K, depending on the mode. Cooling the sample below 30 K leads to a hysteresis between curves measured during cooling/heating. Both effects can be taken as evidence for a coupling of the lattice to spin degrees of freedom. In Figure 7 we show corresponding data of

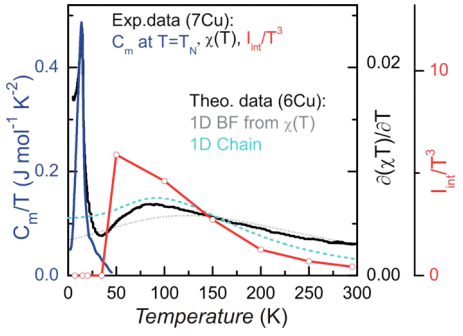

Figure 7. Magnetic specific heat, C_m/T, of $Cu_7(TeO_3)_6F_2$ in the intermediate to high-temperature regime derived from the Raman scattering continuum (red curve), the Fisher specific heat from $\chi \cdot T$ (black line, experiment; dotted gray, Bonner–Fischer model), and a calculation of the specific heat of a spin chain (dashed light blue), see text. The measured magnetic specific heat at T_N is shown for comparison (dark blue).

$I_{Int}(T)/T^3$ together with other measures related to the specific heat, C_p/T. The quasielastic Raman scattering data leads to a broad maximum with a sharp drop for $T < 50$ K. The measured magnetic susceptibility can be used to determine the so-called Fisher specific heat. We use the expression $C_p(T) \propto \partial(\chi \cdot T)/\partial T$.[35,36] This data shows a broader maximum with a decrease for $T < 75$ K. Finally we compare this data with the modeling of the specific heat of an infinitely long chain of spins.[37] The latter

dx.doi.org/10.1021/ic5009686 | Inorg. Chem. 2014, 53, 7661−7667

data shows a very broad maximum ($T_{max} \propto 0.3 \cdot J_{AFM}$) and an even weaker decrease at lower temperatures.

It is noticeable that the calculated specific heat of a spin chain does not show a decrease even at lowest temperatures. This constant specific heat is due to strong quantum fluctuations of the spin chain as long as long-range ordering is prohibited. In contrast, the experimental observations show a different picture. Here it depends on the measure whether contributions at low temperature are detected or not. In the Raman scattering data a rather discontinuous suppression is observed for $T < 50$ K. In this temperature range the directly measured specific heat evidenced a loss of magnetic entropy corresponding to one $S^{eff} = {}^1/_2$ moment. In good agreement with the previous discussion of the magnetic susceptibility, this can be taken as evidence that two subsystems of magnetic degrees of freedom exist: one system shows a large antiferromagnetic exchange coupling with continuous fluctuations, nearly independent of temperature and a second system with a smaller coupling. The latter one is involved in long-range ordering. For the consideration of the microscopic mechanism that leads to the suppression of fluctuations in the chain, two origins are considered. First, the weakly interacting spin moments could induce local fields at the connections to the spin chains. These can effectively increase the dimensionality and connect the chains. Second, local lattice distortions may induce changes of the exchange coupling; e.g., a cutting of the chains can effectively enhance tendencies for long-range ordering.

In the following we will analyze and discuss the magnetic exchange topology. In the given Cu-coordinations, the connectivities to fluorine ions are irrelevant as they are always terminal. Therefore, we consider exclusively Cu−O−Cu bonds. Here only one relevant magnetic orbital state on the Cu ion, either $d_{x^2-y^2}$ or d_{z^2}, respectively, with overlap to oxygen p-states can induce superexchange. According to the Goodenough−Kanamori rules[38] the strength of this exchange is strongly depending on the bond angle. Following this route we notice that the exchange topology is by far not three- or two-dimensional. In contrast, chains along [110] exist that are formed by Cu ions with large exchange coupling based on the Cu−O−Cu angles larger than 100°. These chains contain Cu(1) (1×), Cu(2) (2×), and Cu(3) (2×). This corresponds to five Cu ions that are all coordinated in distorted plaquets with $d_{x^2-y^2}$ magnetic orbitals. Attached to these chains are two Cu(4) which are considerably different from the previous coordinations, namely trigonal-bipyramidal, which alters the single-ion ground state to be associated with a d_{z^2} magnetic orbital. Importantly, these Cu(4) atoms do not connect to an adjacent Cu(4) through common magnetic orbitals, but rather via a $d_{z^2}-(d_{x^2-y^2}, d_{xy})$ arrangement with the latter set of nonmagnetic character. In this way these ions play the role of "loose ends". In Figure 8 we sketch the corresponding magnetically relevant coordinations.

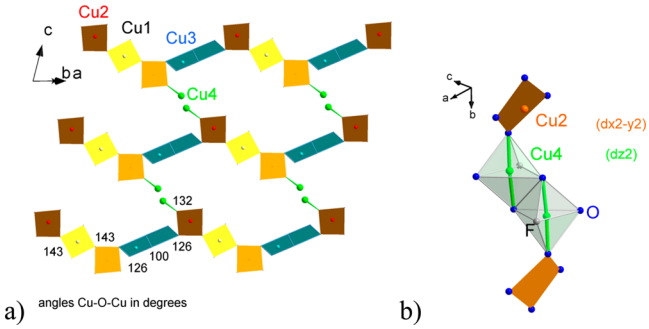

Figure 8. (a) Sketches of the exchange topology in $Cu_7(TeO_3)_6F_2$ that forms spin chains along [110]. The numbers give the Cu−O−Cu angles in degrees. (b) "Loose ends" are formed by two Cu(4) with d_{z^2} orbitals. Note that the joint edges do not couple with respect to superexchange.

CONCLUSIONS

The synthesis and crystal structure of a new oxofluoride, $Cu_7(TeO_3)_6F_2$, has been reported. It has been synthesized by hydrothermal synthesis and crystallizes in the triclinic system, space group $P\bar{1}$. The crystal structure constitutes a framework with channels where the F^- ions and the stereochemically active lone-pairs on Te^{4+} are located. There are four crystallographic Cu atoms having different coordinations. The F^- ion only forms one bond and is a terminating ion in the crystal structure; this is uncommon as fluorine tends to be a bridging ion in oxofluorides. The three crystallographically different Te^{4+} ions have one-sided $[TeO_3]$ and $[TeO_5]$ coordinations that polymerize to form unusual $[Te_3O_9E_3]$ trimers for which ELF-calculations indicate that the stereochemically active lone-pair has its highest electron density 0.9−1.0 Å away from the Te^{4+} ions.

The structure description indicates that the three-dimensional framework consists of Cu−O connections. However, an evaluation of the relevant magnetic Cu-orbitals reveals a strongly reduced dimensionality. On the basis of thermodynamic and Raman scattering data, for temperatures above ≈75 K we derive a scenario of chains with dominant antiferromagnetic exchange (J_{AFM} = 290 K) that are weakly coupled to "loose end" members. The latter give rise to residue moments ($S^{eff} = {}^1/_2$) which eventually initiate the long-range ordering at $T_N \approx 15$ K. It is noteworthy that this ordering process is also accompanied by presumably structural distortions as indicated by the temperature dependence of several phonon modes upon cooling and heating cycles.

ASSOCIATED CONTENT

Supporting Information

Atomic coordinates, selected interatomic distances (Å) and angles (deg), results from bond valence sum (BVS) calculations, and EDS-analysis for $Cu_7(TeO_3)_6F_2$. Crystallographic data in CIF format. This material is available free of charge via the Internet at http://pubs.acs.org.

AUTHOR INFORMATION

Corresponding Author

*E-mail: mats.johnsson@mmk.su.se. Phone: +46-8-162169. Fax: +46-8-152187.

Notes

The authors declare no competing financial interest.

ACKNOWLEDGMENTS

This work has in part been carried out through financial support from the Swedish Research Council. A.M. acknowledges support from the Texas Center for Superconductivity and the National Science Foundation (Grant DMR-1149899). P.L. acknowledges support from the NTH School *Contacts in Nanosystems*.

REFERENCES

(1) Galy, J.; Meunier, G.; Andersson, S.; Astrom, A. *J. Solid State Chem.* **1975**, *13*, 142−159.
(2) Seshadri, R.; Hill, N. A. *Chem. Mater.* **2001**, *13*, 2892−2899.
(3) Ok, K. M.; Halasyamani, P. S. *Angew. Chem., Int. Ed.* **2004**, *43*, 5489−5491.
(4) Johnsson, M.; Törnroos, K. W.; Mila, F.; Millet, P. *Chem. Mater.* **2000**, *12*, 2853−2857.
(5) Johnsson, M.; Törnroos, K. W.; Lemmens, P.; Millet, P. *Chem. Mater.* **2003**, *15*, 68−73.
(6) Becker, R.; Johnsson, M.; Kremer, R. K.; Klauss, H.-H.; Lemmens, P. *J. Am. Chem. Soc.* **2006**, *128*, 15469−15475.
(7) Takagi, R.; Johnsson, M.; Gnezdilov, V.; Kremer, R. K.; Brenig, W.; Lemmens, P. *Phys. Rev.* **2006**, *B74*, 014413.
(8) Jiang, H.-L.; Mao, J.-G. *Inorg. Chem.* **2006**, *45*, 7593−7599.
(9) Zhang, D.; Berger, H.; Kremer, R. K.; Wulferding, D.; Lemmens, P.; Johnsson, M. *Inorg. Chem.* **2010**, *49*, 9683−9688.
(10) Lemmens, P.; Choi, K. Y.; Kaul, E. E.; Geibel, C.; Becker, K.; Brenig, W.; Valenti, R.; Gros, C.; Johnsson, M.; Millet, P.; Mila, F. *Phys. Rev. Lett.* **2001**, *87*, 227201−1.
(11) Pregelj, M.; Zaharko, O.; Zorko, A.; Kutnjak, Z.; Jeglic, P.; Brown, B. P.; Jagodic, Z.; Berger, H.; Arcon, D. *Phys. Rev. Lett.* **2009**, *103*, 147202(4).
(12) Laval, J. P.; Boukharrata, N. J.; Thomas, P. *Acta Crystallogr.* **2008**, *C64*, i12−i14.
(13) Laval, J. P.; Boukharrata, N. J. *Acta Crystallogr.* **2008**, *C64*, i57−i61.
(14) Laval, J. P.; Boukharrata, N. J. *Acta Crystallogr.* **2009**, *C65*, i1−i6.
(15) Boukharrata, N. J.; Duclère, J. R.; Laval, J. P.; Thomas, P. *Acta Crystallogr.* **2013**, *C69*, 460−462.
(16) Hu, S.; Johnsson, M. *Dalton Trans.* **2012**, *41*, 12786−12789.
(17) *CrysAlisCCD and CrysAlisRED*; Oxford Diffraction Ltd.: Abingdon, U.K., 2006.
(18) Sheldrick, G. M. *Acta Crystallogr.* **2008**, *A64*, 112−122.
(19) Koichi, M.; Fujio, I. *J. Appl. Crystallogr.* **2011**, *44*, 1272−1276.
(20) Brown, I. D.; Altermatt, D. *Acta Crystallogr.* **1985**, *B41*, 244−247.
(21) www.cp2k.org (visited 2014-04-07).
(22) Lippert, G.; Hutter, J.; Parrinello, M. *Physica* **1997**, *92*, 477−487.
(23) Goedecker, S.; Teter, M.; Hutter, J. *Phys. Rev. B* **1996**, *54*, 1703−1710.
(24) Grimme, S.; Antony, J.; Ehrlich, S.; Krieg, H. *J. Chem. Phys.* **2010**, *132*, 154104.
(25) Bain, G. A.; Berry, J. F. *J. Chem. Educ.* **2008**, *85* (4), 532−536.
(26) Katsumata, T.; Nakashima, M.; Umemoto, H.; Inaguma, Y. *J. Solid State Chem.* **2008**, *181*, 2737−2740.
(27) Needs, R. L.; Dann, S. E.; Weller, M. T.; Cherryman, J. C.; Harris, R. K. *J. Mater. Chem.* **2005**, *15*, 2399−2407.
(28) Akopjan, A. V.; Serov, T. V.; Dolgikh, V. A.; Ardashnikova, E. I.; Lightfoot, P. *J. Mater. Chem.* **2002**, *12*, 1490−1494.
(29) Hu, S.; Johnsson, M. *Dalton Trans.* **2013**, *42*, 7859−7862.
(30) Hugonin, Z.; Johnsson, M.; Lidin, S.; Wulferding, D.; Lemmens, P.; Kremer, R. K. *J. Solid State Chem.* **2008**, *181*, 2776−2782.
(31) Brown, I. D. *The Chemical Bond in Inorganic Chemistry: The Bond Valence Model*; Oxford University Press: New York, 2002.
(32) Bonner, J. C.; Fisher, M. E. *Phys. Rev.* **1964**, *135*, A640−A658.
(33) Lemmens, P.; Fischer, M.; Güntherodt, G.; Gros, C.; van Dongen, P. G. J.; Weiden, M.; Richter, W.; Geibel, C.; Steglich, F. *Phys. Rev. B* **1997**, *55*, 15076−15083.
(34) Lemmens, P.; Güntherodt, G.; Gros, C. *Phys. Rep.* **2003**, *375*, 1−103.
(35) Fisher, M. E. *Philos. Mag.* **1962**, *7*, 1731−1743.
(36) Aharen, T.; Greedan, J. E.; Ning, F.; Imai, T.; Michaelis, V.; Zhou, H.; Wiebe, C. R.; Cranswick, L. M. D. *Phys. Rev. B* **2009**, *80*, 134423.
(37) Klumper, A.; Johnston, D. C. *Phys. Rev. Lett.* **2000**, *84*, 4701−4704.
(38) Anderson, P. W. *Solid State Phys.* **1963**, *14*, 99−214.

dx.doi.org/10.1021/ic5009686 | *Inorg. Chem.* 2014, 53, 7661−7667